ACS APPLIED ENGINEERING MATERIALS

pubs.acs.org/acsaenm Article

Engineering of an Isoreticular Series of CALF-20 Metal−Organic Frameworks for CO_2 Capture

Karuppasamy Gopalsamy, Dong Fan, Supriyo Naskar, Yann Magnin, and Guillaume Maurin*

Cite This: ACS Appl. Eng. Mater. 2024, 2, 96−103 Read Online

ACCESS | Metrics & More | Article Recommendations | Supporting Information

ABSTRACT: A series of linker-substituted ultramicroporous CALF-20 metal−organic frameworks (MOFs) were built in silico, and their CO_2 capture performances over N_2 in flue gas conditions were systematically computationally explored. Among the various linker substitutions explored, squarate-linker-incorporated CALF-20 (SquCALF-20) was demonstrated to show a larger CO_2 uptake at 0.15 bar (3.6 mmol/g) and higher CO_2/N_2 selectivity (500) in dry conditions compared to pristine CALF-20. Interestingly, this MOF was shown to maintain a high level of CO_2 capture performance even in the presence of humidity, although it starts to adsorb H_2O at lower relative humidity compared to CALF-20. Because squaric acid is a semiconductor industry feedstock and the few-already published squarate-based MOFs are chemically robust, this engineered SquCALF-20 offers a promising avenue for cost-effective CO_2 capture via physisorption, with potential applications in addressing environmental concerns associated with CO_2 emissions.

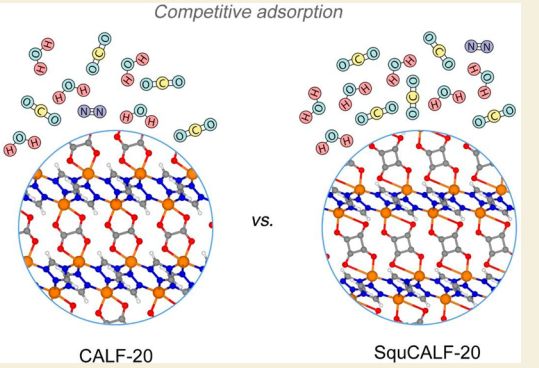

KEYWORDS: *CALF-20, MOF, in silico structure engineering, CO_2 capture, flue gas, molecular simulations*

INTRODUCTION

CO_2 emissions into the atmosphere warm the planet, causing climate change and serious related health issues.[1] Aqueous amine-based CO_2 absorption technology is mature for postcombustion capture of CO_2 emitted from power plant exhaust gases; however, it raises concerns in terms of toxicity and implies a high energy-cost regeneration process.[2] Physisorption-based processes using porous sorbents are a valuable alternative strategy to achieve energetically effective CO_2 capture.[3] Beyond the emblematic porous sorbents, including activated carbons,[4] mesoporous silica,[5] and zeolites,[6] metal−organic frameworks (MOFs),[7] one of the most recent classes of porous crystalline solids, have attracted tremendous interest for diverse adsorption/separation applications due to their unprecedented chemical versatility and high tunability of their pore size/shape. A myriad of MOFs has been proposed over the last 2 decades with promising performance for CO_2 capture[7−12] that paves the way toward alternative solutions to the standard CO_2 zeolite sorbents.[6] The ultramicroporous SIFSIX-3-M (M = Zn and Cu) is one of the first prominent CO_2 sorbent MOFs exhibiting very high CO_2/N_2 selectivity, i.e., SIFSIX-3-Cu (10500) and SIFSIX-3-Zn (7250) associated with relatively large CO_2 uptakes (1.24 and 0.13 mmol/g, respectively) at 400 ppm and 298 K.[13] The hydrolytically stable fluorinated MOF **NbOFFIVE**-1-Ni (KAUST-7) derived from the same MOF platform was further demonstrated to be an excellent candidate for CO_2 capture directly from air (direct air capture) combining high CO_2 amount adsorbed at traces (1.3 mmol/g at 400 ppm and 298 K) and reasonable regeneration energy cost.[14] Long et al. reported the *N,N*-dimethylethylenediamine-functionalized Mg_2(dobpdc) MOF structure for CO_2 capture from air/flue gas (CO_2, N_2, and O_2).[15] This MOF was demonstrated to show very high CO_2 uptake of 2.0 mmol/g at 0.00039 bar and 298.15 K (air capture) and 3.1 mmol/g at 0.15 bar and 313.15 K (flue gas) associated with very high CO_2/N_2 selectivity of up to 49000.

However, some of these potential CO_2 sorbent MOFs suffer from competitive adsorption of H_2O, which leads to a substantial drop of CO_2 sorption capacity under the operating humidity conditions and/or a costly regeneration process with the use of relatively high-temperature treatment and still some issues in terms of long-term stability.[16−18] To overcome these shortcomings, Shimizu et al.[19] recently proposed a highly thermal and chemically robust zinc triazolate MOF made of 1,2,4-triazolate-bridged zinc(II) layers pillared by the oxalate ligand [Zn_2(1,2,4-triazolate)$_2$(oxalate)], namely, CALF-20 (CALF stands for Calgary Framework), seen as the current

Received: October 10, 2023
Revised: December 13, 2023
Accepted: December 13, 2023
Published: January 8, 2024

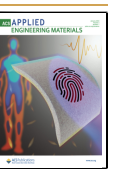

benchmark MOF sorbent for CO_2 capture from cement flue gas. This material encompasses an excellent CO_2/N_2 selectivity of 230 and large CO_2 uptake in postcombustion conditions (2.8 mmol/g at 0.15 bar and 293 K) combined with high durability and relatively easy scalability.[19] Interestingly, this level of performance was demonstrated to be maintained in the presence of moisture up to 25% relative humidity (RH) once the MOF is shaped with a polysulfone binder. The shaping of this MOF has also been recently computationally explored.[45] More generally, the promise of zinc triazolate-based MOFs for CO_2 capture has been widely discussed in the literature, including $Zn_2(Atz)_2(ox)$ (Atz = 3-amino-1,2,4-triazole; ox = oxalate).[20] A series of zinc triazolatedicarboxylate pillar-layered MOFs has been constructed with dicarboxylate linkers of different lengths and functional groups.[21] Recently, Li et al. systematically engineered the pillaring of zinc triazolate layers with benzenedicarboxylate linkers and their ortho functionalized derivatives, e.g., Bdc-F, Bdc-Cl, Bdc-NH_2, Bdc-NO_2, and Bdc-CH_3, to tune the CO_2 sorption uptake of the resulting MOFs at 1 bar,[22] while Wang et al. proposed cobalt triazolate-based MOFs with biphenyldicarboxylate linker units for the same target.[23]

Inspired by these findings, herein, we deliberately expand the CALF-20 platform by envisioning an isoreticular series of MOFs with substitution of the oxalate ligand of the parent CALF-20 by alternative small linkers, including squarate (Squ), fumarate (Fum), benzenedicarboxylate (Bdc), thieno[3,2-*b*]thiophene-2,5-dicarboxylate (Ttdc), and cubanedicarboxylate (Cub). Note that these linkers have already been used as building units to synthesize many MOFs. Their CO_2 capture performance over N_2 under dry and humid conditions was further computationally assessed to predict alternative MOFs with even better performances than CALF-20 to further guide experimental efforts toward their synthesis and testing. SquCALF-20 was identified as the best candidate, combining high CO_2 uptake at 0.15 bar (3.6 mmol/g) and very high CO_2/N_2 selectivity (500), exceeding the performance of pristine CALF-20 while maintaining this attractive level of CO_2 adsorption performance under moderate moisture.

COMPUTATIONAL METHODS

Density Functional Theory (DFT) Calculations

The crystal structures of pristine CALF-20 and its engineered derivatives constructed by substituting the pristine oxalate linker with Squ, Fum, Bdc, Ttdc, and Cub were fully geometry-optimized (atomic positions and cell parameters relaxed) at the periodic DFT level without imposing any constraints in terms of topology/geometry. These calculations were performed using the *Quickstep* module[24] of the *CP2K* program[25] with the Gaussian plane-wave formalism. The Perdew–Burke–Ernzerhof[26] functional combined with Grimme's DFT-D3 semiempirical dispersion corrections was used for all calculations.[27,28] All atoms except Zn were modeled via triple-ζ plus valence-polarized Gaussian-type basis sets (TZVP-MOLOPT), while for Zn, double-ζ plus valence polarization functions (DZVP-MOLOPT) were employed.[29] Core electron–valence shell interactions were described by the norm-conserving pseudopotentials proposed by Goedecker, Teter, and Hutter.[30−32] The energy cutoff for the plane-wave basis set was set to 500 Ry. The atomic partial charges for each MOF were calculated using the repeating electrostatic potential extracted atomic (REPEAT) charge[33] method for further Monte Carlo (MC) and molecular dynamics (MD) simulations.

Grand Canonical Monte Carlo (GCMC) Simulations

CO_2 single-component and CO_2/N_2 (15:85) binary mixture adsorption isotherms were simulated for all MOFs at 293 K using GCMC calculations, as implemented in the Complex Adsorption and Diffusion Simulation Suite (CADSS) code.[34] For pristine CALF-20 and the derivatives showing the best CO_2 sorption performance, H_2O single-component and $CO_2/N_2/H_2O$ ternary mixture adsorption isotherms were further computed. Several types of Monte Carlo moves were considered: translation move, rotation move, and insertion/deletion move. The frequencies of these moves were 0.3, 0.3, 0.2, and 0.2, respectively. In the case of a mixture, a molecular exchange move was additionally considered. A simulation box consisting of 27 unit cells (3 × 3 × 3) was considered for all MOFs, and the atomic positions of the MOFs were held fixed during the simulations. The host–guest nonbonded interactions were treated as the sum of a van der Waals interaction term and a Coulombic contribution. The Lennard–Jones (LJ) interactions were computed with a cutoff of 12.0 Å, while the electrostatic interactions were calculated using the Ewald summation[35] technique with an accuracy of 1×10^{-6}. The parameters for all MOF atoms were taken from the DREIDING[36] force field, and their atomic partial charges were DFT-derived using the REPEAT scheme.[33] CO_2 was described by a three-site charged LJ model as defined by Garcia-Sánchez et al.,[37] and N_2 was represented by a three-site charged model, with two LJ sites located at the N atoms while a third site present at its center of mass only involves electrostatic interactions.[38] H_2O was modeled as a four-site TIP4P_Ew model.[39] Table S1 provides the LJ parameters and atomic partial charges for all atoms. The LJ cross-term parameters were obtained by applying the Lorentz–Berthelot mixing rules.[40] For each pressure point, 2×10^7 and 2×10^8 Monte Carlo production steps following 10^7 and 10^8 Monte Carlo equilibration steps were considered for the CO_2 single component/binary mixture and the H_2O single component/ternary mixture, respectively. The Peng–Robinson equation of state was used to determine the gas-phase fugacity.[41] The simulated single-component water adsorption isotherm for CALF-20 was first compared to both previous calculations and the corresponding experimental data.[19] This comparison is reported in Figure S1. One can observe that our simulations reproduce very well the experimental S-shaped adsorption isotherm up to 20% RH, while they overestimate the amount adsorbed between 30% and 80% RH and match the experimental saturation uptake. Notably, these simulations led to a better agreement with the experimental data compared to the previous simulation work using a different force field to describe the H_2O/CALF-20 interactions.[19] This overall agreement between the simulated and experimental water adsorption isotherms enabled evidence that the selected force field for both H_2O and CALF-20 atoms along the MOF partial charges achieve a fair description of the host/guest interactions in this system.

The radial distribution functions (RDFs) for all MOF/guest atom pairs were averaged over the Monte Carlo steps at different pressure ranges. The adsorption enthalpies for CO_2 and N_2 were calculated for all MOFs at infinite dilution $\Delta H_{ads,\theta=0}$ using the Widom insertion method,[42] while the corresponding values for H_2O were calculated only for CALF-20 and SquCALF-20. The adsorption enthalpy for CO_2 was also calculated by GCMC simulations as a function of the CO_2 uptake.

MD Simulations

Single-component CO_2 diffusion was investigated in CALF-20 and its best CO_2-sorbent derivatives at 293 K for a typical loading of 1 CO_2 molecule/unit cell. These MD simulations were performed using the Large-scale Atomic/Molecular Massively Parallel Simulator (LAMMPS)[43] simulation package. In the MD simulations, CALF-20 and the best CO_2-sorbent framework moieties were treated as flexible. In these calculations, the parameters for the intramolecular bonding, bending, and dihedral terms of the MOFs were taken from the UFF force field[44] since it was successfully applied to describe the flexibility of the pristine CALF-20 structure,[45] while the DREIDING[36] parameters were selected to define the nonbonded LJ

https://doi.org/10.1021/acsaenm.3c00622
ACS Appl. Eng. Mater. 2024, 2, 96−103

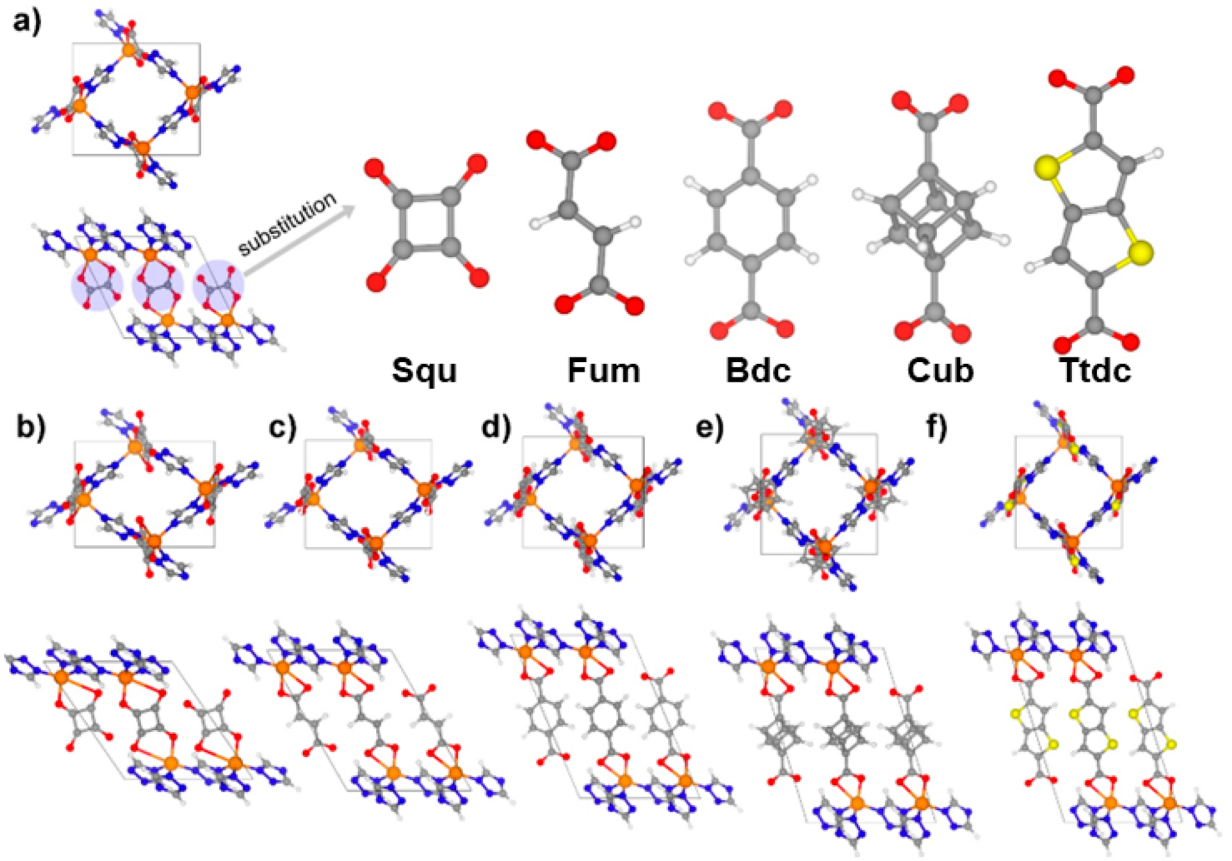

Figure 1. Illustration of the DFT-optimized structures of CALF-20 (a) and its derivatives SquCALF-20 (b), FumCALF-20 (c), BdcCALF-20 (c), TtdcCALF-20 (d), and CubCALF-20 (e). The resulting cell parameters are provided for all MOFs in Table S2. Color code: red, O; gray, C; white, H; yellow, S; orange, Zn.

potentials in a manner similar to that of the GCMC simulations. All of these simulations were performed in the *NVT* ensemble for 200 ns production runs following 20 ns equilibration and a time step of 1 fs. The Nosé–Hoover thermostat[46] was employed to maintain the temperature with a coupling constant time of 0.5 ps. The self-diffusion coefficients (D_s) of CO_2 averaged over three MD trajectories were calculated by applying Einstein's diffusion relationship to the linear region of the MSD versus time plot.

RESULTS AND DISCUSSION

Figure 1 illustrates the DFT-optimized crystal structures of CALF-20 and its derivatives, SquCALF-20, FumCALF-20, BdcCALF-20, TtdcCALF-20, and CubCALF-20. The structural information and textural properties of this isoreticular series of MOFs, including the pore volume (PV), void fraction (ϕ), largest cavity diameter, and pore-limiting diameter (PLD) assessed by using the *Zeo++* software,[47] are tabulated in Table S2. PLD ranges from 2.7 Å (CubCALF-20) to 3.0 Å (FumCALF-20), while PV varies from 0.32 cm^3/g (CALF-20) to 0.49 cm^3/g (BdcCALF-20). As shown in Figure 1b–f, the organic ligand with incremental length increases the 1D channel pore dimension of the pristine CALF-20 (see also Table S2).

Single-Component CO_2 Adsorption

We further validated the selected force-field parameters and atomic partial charges of the MOFs alongside the models used for CO_2 by an excellent agreement between the CO_2 adsorption isotherm simulated for CALF-20 at 293 K with the corresponding experimental data reported previously[19] in the pressure domain of 0–1 bar (Figure 2a).

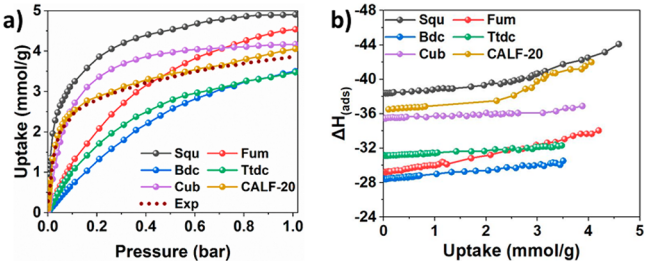

Figure 2. GCMC-predicted (a) single-component CO_2 adsorption isotherms and (b) adsorption enthalpy for CALF-20 and its derivatives in the pressure range of 0–1 bar at 293 K. The experimental data from ref19 are incorporated in part a for comparison.

The CO_2 adsorption isotherms further simulated for all CALF-20 derivatives evidenced that the choice of the linker enables to tune the CO_2 sorption uptake in the overall range of pressure explored, as shown in Figure 2a. Typically, at 1 bar the sequence BdcCALF-20 ~ TtdcCALF-20 (3.5 mmol/g) < CALF-20 (4.1 mmol/g) < CubCALF-20 (4.2 mmol/g) < FumCALF-20 (4.5 mmol/g) < SquCALF-20 (4.9 mmol/g) is revealed, while at 0.15 bar, SquCALF-20 (3.6 mmol/g) and to a lesser extent CubCALF-20 (3.1 mmol/g) still outperform CALF-20 (2.8 mmol/g). Analysis of the CO_2 distribution

https://doi.org/10.1021/acsaenm.3c00622
ACS Appl. Eng. Mater. 2024, 2, 96–103

(Figure S2) in the pores of SquCALF-20 (PLD = 2.9 Å; PV = 0.35 cm^3/g) evidenced that a tiny expansion of its pore size/pore volume compared to CALF-20 (PLD = 2.8 Å; PV = 0.32 cm^3/g) favors the adsorption of a large concentration of CO_2 in the low domain of pressure (Figure 2a). This is in line with a slightly higher simulated adsorption enthalpy at low coverage for SquCALF-20 (−38.4 kJ/mol) compared with CALF-20 (−36.5 kJ/mol) and other MOF derivatives (Figure 2b). Enhancement of the adsorption enthalpy with CO_2 uptake is attributed to an increase of the CO_2/CO_2 interaction energy contribution, as highlighted in Figure S3. Analysis of the RDF calculated for the most significant CO_2/MOF atom pairs (Figure S4a,b) for both SquCALF-20 and CALF-20 at 0.15 bar pressure revealed that while CO_2 interacts similarly with both the O atoms of the oxalate groups and the H atoms of the triazolate linkers [almost similar mean separating $O_{oxalate}-C_{CO_2}$ (3.3 Å) and $H_{triazolate}-C_{CO_2}$ (3.7 Å) distances and the same peak intensities] in CALF-20, the situation differs for SquCALF-20, where CO_2 preferentially interacts with the O atoms of the squarate group (mean separating $O_{squarate}-C_{CO_2}$ distance of 3.0 Å) and to a lesser extent with the atoms of the triazolate linkers. Figure 3 illustrates the adsorption configurations for CO_2 in both CALF-20 materials, evidence that the preferential interactions of CO_2 with the squarate O atoms in SquCALF-20 is made possible by the fact these adsorption sites are pointing toward the pore center and they are therefore more accessible for the guest molecules.

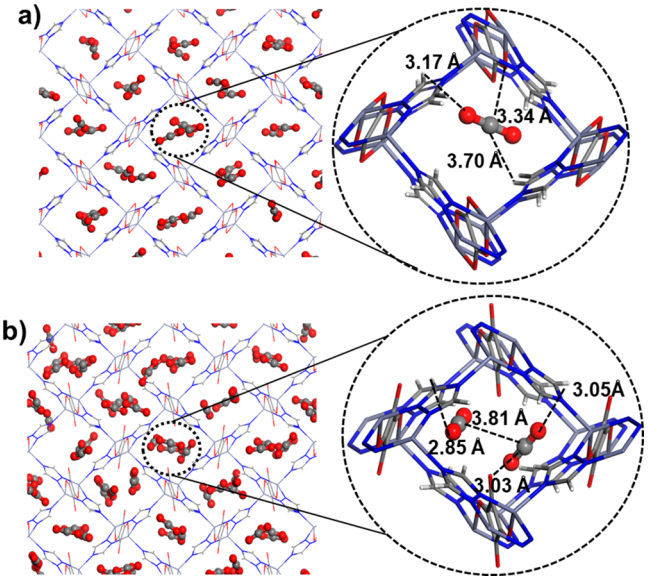

Figure 3. Illustration of the preferential sittings of CO_2 obtained from the single-component Monte Carlo simulations at 0.15 bar along their characteristic interacting distances in (a) CALF-20 and (b) SquCALF-20. For a better view, a single unit cell of each MOF structure is presented as an inset, with CALF-20 and SquCALF-20 adsorbing 1 CO_2 molecule/unit cell and 2 CO_2 molecules/unit cell at this pressure, respectively.

This favors a more effective packing of CO_2 in the pores of SquCALF-20, and hence combined with a slightly higher PV of this MOF compared to CALF-20, this leads to an enhancement of the CO_2 loading at a given pressure, e.g., 1 and 2 CO_2 molecules/unit cell for CALF-20 and SquCALF-20 at 0.15 bar, respectively. This is illustrated in the Monte Carlo snapshots provided in Figure S5a,b. The RDF plots calculated for the $C_{CO_2}-C_{CO_2}$ pairs in CALF-20 and SquCALF-20 (Figure S5c,d) exhibit similar profiles, with a first peak in the range of 3.4−3.6 Å in line with the high confinement of CO_2 in the MOF pores.

Binary CO_2/N_2 Mixture Adsorption

CO_2/N_2 (15:85) binary mixture GCMC simulations were performed for the full series of isoreticular CALF-20 MOFs to further assess their promises for CO_2 capture from flue gases. Figure 4a reports the corresponding adsorption isotherms, while Table S3 summarizes the CO_2 uptakes calculated at different total pressures for the mixture compared to the scenario of the CO_2 single component.

These simulated data evidence that SquCALF-20 still adsorbs the largest amount of CO_2 at low pressure in mixture. This, combined with a very low N_2 adsorbed amount (Figures 4a and S6), translates into a CO_2/N_2 selectivity at 1 bar above 500, substantially higher than the value simulated for CALF-20 (180) and all other derivatives including CubCALF-20 (78), as shown in Figure 4b. This behavior is in line with the highest simulated adsorption enthalpy at low coverage difference obtained between CO_2 and N_2 for SquCALF-20 compared to the other MOFs (Table S4 and Figure S7), with the calculated adsorption enthalpy at low coverage difference between CO_2 and N_2 evolving as follows: −17.8 kJ/mol (SquCALF-20) > −15.4 kJ/mol (CALF-20) > −15.0 kJ/mol (CubCALF-20) > −13.0 kJ/mol (TtdcCALF-20) > −12.9 kJ/mol (FumCALF-20) > −12.2 kJ/mol (BdcCALF-20). Figure 4c shows that the CO_2 molecules are distributed in mixture conditions in a manner similar to that of a single component with only a minor concentration of N_2 molecules adsorbed. Analysis of the RDFs calculated for the most significant CO_2/MOF atom pairs (Figure S6a,b) for both SquCALF-20 and CALF-20 for the binary mixture at a total pressure of 1 bar revealed that CO_2 adopts the same adsorption mode as that in the single-component scenario (Figure S4a,b), with a preferential sitting of CO_2 toward the O atoms of the squarate groups for SquCALF-20 leading to a better packing of CO_2 in its pore and an optimum CO_2 selectivity over N_2.

CO_2/N_2 Separation Performance in the Presence of Humidity

As a further step, we explored the ternary adsorption of the $CO_2/N_2/H_2O$ ternary mixture in CALF-20 and SquCALF-20 at 293 K as well as the single-component H_2O adsorption in these two MOFs for comparison. These calculations were performed using a representative $CO_2/N_2/H_2O$ ternary mixture composition of 0.199995324:0.799981296:0.00023380 for 1% RH, while a total pressure of 1 bar was applied (see Table S5 for the ternary mixture molar fraction for each % RH). The corresponding data are reported in Figure 5a,b. The calculated single-component H_2O distribution snapshots at different RHs and the corresponding RDF plots for water−MOF and water−water pairs in CALF-20 and SquCALF-20 are shown in Figures S8 and S9, respectively. This analysis shows that the H_2O adsorption mechanism is similar in both the SquCALF-20 MOF and pristine CALF-20.

SquCALF-20 is found to be more hydrophilic than CALF-20 starting to adsorb H_2O at lower RH (Figure 5a,b) in line with a slightly higher calculated adsorption enthalpy for H_2O at low coverage (−38.7 vs −33.4 kJ/mol, respectively). Analysis of the snapshots evidences that CO_2 preferentially adsorbs in the center of the MOF cavities while H_2O molecules are closer to

https://doi.org/10.1021/acsaenm.3c00622
ACS Appl. Eng. Mater. 2024, 2, 96−103

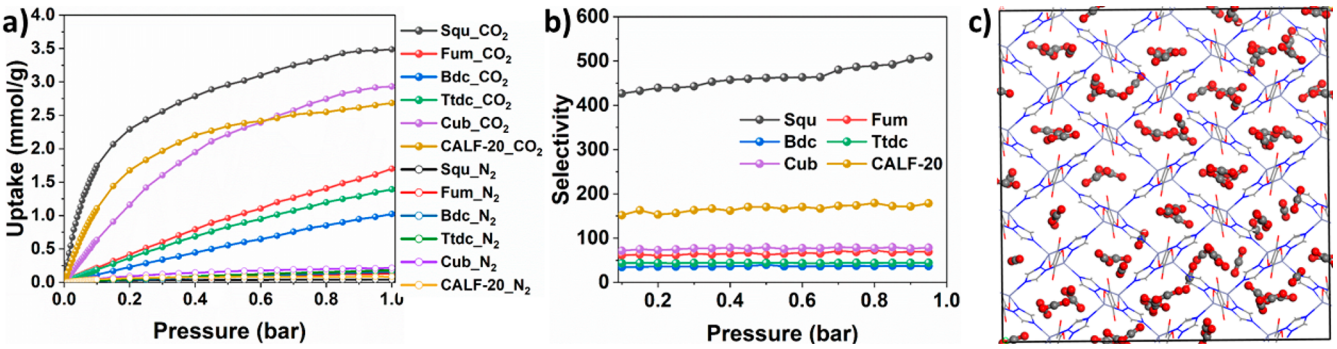

Figure 4. GCMC-simulated CO_2/N_2 (15:85 composition) mixture (a) adsorption isotherms and (b) selectivity in the pressure range from 0 to 1 bar at 293 K [the selectivity for CO_2 over a N_2 gas molecule is calculated using the expression $S\left(\frac{CO_2}{N_2}\right) = \left(\frac{X_{CO_2}}{X_{N_2}}\right)\left(\frac{Y_{CO_2}}{Y_{N_2}}\right)$, where X_{CO_2} and X_{N_2} are the molar fractions of CO_2 and N_2 gas molecules in the adsorbed phase, while Y_{CO_2} and Y_{N_2} are the molar fractions of CO_2 and N_2 molecules in the bulk phase, respectively]. (c) Simulated snapshot of a CO_2/N_2 mixture in SquCALF-20 at a total pressure of 1 bar (viewed along the MOF 1D channel pore).

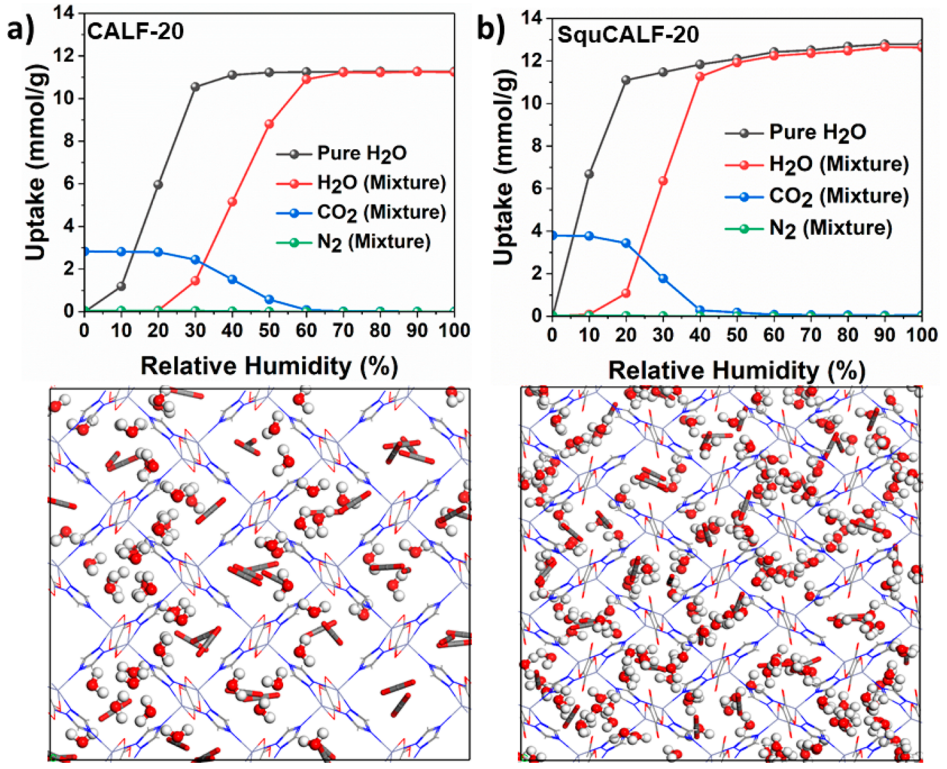

Figure 5. GCMC-simulated $CO_2/N_2/H_2O$ ternary mixture (see Table S5 for the ternary mixture mole fraction for each % RH with a total applied pressure of 1 bar) adsorption isotherms at 293 K along with illustrative snapshots calculated under RHs of 30% and total pressures of the system kept at 1 bar for (a) CALF-20 and (b) SquCALF-20. CO_2 is represented as rodlike molecules, and H_2O is shown as ball−stick representations.

the pore wall (Figure 5a). Indeed, because the affinity of SquCALF-20 for H_2O is very similar to that for CO_2 (−38.4 kJ/mol), adsorption of CO_2 is still favored at low RH in the same location as in the scenario of the single component. Decisively, SquCALF-20 maintains its larger CO_2 sorption capacity of 3.4 mmol/g (vs 2.7 mmol/g for CALF-20) up to RH = 20% and shows a decrease above with a sorption uptake of 1.8 mmol/g at RH = 30%. At this RH = 30% and above, H_2O molecules preferentially adsorb in the vicinity of the O atom of squarate ($O_{squarate}$), with the formation of relatively strong hydrogen bonds associated with a separating distance of 1.7 Å (see the corresponding RDF in Figure S10a,b) while forming an extended strong hydrogen-bond network (Figure S10c) at higher RH associated with a high-intensity peak for the $H_{water}-O_{water}$ pair at 1.8 Å. A similar hydrogen-bond network (from water cluster multimers to wired hydrogen-bond network structures) was reported for CALF-20 recently by Magnin et al.[48] This water organization constrains CO_2 molecules to occupy only the pore center of SquCALF-20 in a manner similar to that in the scenario of CALF-20 (see the snapshot in Figure 5a,b) and therefore leads to a gradual reduction of the CO_2 uptake for RH > 30%. A similar adsorption mechanism of CO_2 under water humidity (with the ranges of % RH) in pristine CALF-20 was also reported recently.[48−50] These studies evidenced (i) the association of H_2O in the vicinity of the CALF-20 pore wall through

https://doi.org/10.1021/acsaenm.3c00622
ACS Appl. Eng. Mater. 2024, 2, 96−103

hydrogen bonds with the MOF atoms and (ii) the formation of water−water hydrogen bonds that repels CO_2 molecules in the middle of the confined pore of CALF-20.[48−50]

Single-Component CO_2 Diffusion and MOF Formation Energy

MD simulations were further performed to assess D_s of CO_2 in CALF-20 and SquCALF-20 at 293 K in the *NVT* ensemble. These calculations revealed that D_s (CO_2) is similar in both MOFs (4.05×10^{-11} and 3.32×10^{-11} m^2/s for CALF-20 and SquCALF-20, respectively; Figure S11), suggesting that the adsorption/desorption kinetics is expected to proceed within the same time scale in both cases. The formation energy of SquCALF-20 and pristine CALF-20 MOFs was further calculated by using DFT calculations to anticipate the stability/synthesizability of the newly engineered MOF. Their resulting calculated formation energies are quite similar, −0.58 and −0.43 eV/atom, respectively. For comparison, Hasan et al. reported an even lower formation energy (−0.18 eV/atom) for the functionalized ZIF8-IR820 that has been successfully synthesized.[51] Therefore, because the formation energy of SquCALF-20 is only slightly lower than that of pristine CALF-20 and much higher than that reported for ZIF8-IR820, this supports that this engineered MOF is synthetically feasible.

CONCLUSIONS

A series of novel ligand-substituted CALF-20 structures were in silico constructed and their CO_2 capture performances were systematically predicted. A SquCALF-20 derivative was demonstrated to show larger CO_2 uptake at 0.15 bar (3.6 mmol/g) and higher CO_2/N_2 selectivity (500) compared to pristine CALF-20. Interestingly, this MOF was shown to maintain a high level of CO_2 performance in the presence of H_2O, although it starts to adsorb H_2O at lower RH compared to CALF-20, while the CO_2 kinetics is expected to be similar to that obtained for CALF-20. It is well documented that squarate-based microporous MOFs are chemically and thermally stable due to the strong bonds formed between squarate O and metal ion,[52] and squaric acid is a semiconductor and laser industry feedstock. This paves the way toward the synthesis of a robust and cost-effective novel ultramicroporous SquCALF-20 highly attractive for CO_2 capture.

ASSOCIATED CONTENT

Supporting Information

The Supporting Information is available free of charge at https://pubs.acs.org/doi/10.1021/acsaenm.3c00622.

MOF atoms and guest molecules force fields (Table S1), lattice parameters and texture properties of studied MOF systems (Table S2), comparison table of CO_2 uptake in a single component and ternary mixture (Table S3), comparison table of the CO_2/N_2 binary mixture heat of adsorption enthalpy (Table S4), ternary mixture $CO_2/N_2/H_2O$ mole fraction composition (Table S5), experimental and simulation comparison graph of single-component H_2O adsorption isotherms (Figure S1), simulation snapshots of CO_2 in CALF-20, SquCALF-20, and CubCALF-20 (Figure S2), different host/guest and guest/guest contributions to the adsorption enthalpies for CO_2 as a single component in CALF-20 and SquCALF-20 (Figure S3), calculated RDF graph of single-component CO_2 in CALF-20 and SquCALF-20 (Figure S4), CO_2 single-component simulation snapshots and CO_2−CO_2 RDFs in CALF-20 and SquCALF-20 at 0.15 and 1 bar (Figure S5a,d), CO_2/N_2 binary mixture simulation snapshots and RDFs in CALF-20 and SquCALF-20 (Figure S6), CO_2/N_2 binary mixture adsorption enthalpy (Figure S7), single-component H_2O adsorption snapshots and RDF in CALF-20 (Figure S8), single-component H_2O adsorption snapshots and RDF in SquCALF-20 (Figure S9), calculated RDF graph of H_2O−SquCALF-20, water−water interaction, and hydrogen-bond formation calculated at 30% RH from a $CO_2/N_2/H_2O$ mixture (Figure S10), calculated CO_2 MSD graph with fitted parameters for CALF-20 and SquCALF-20 structures (Figure S11), and computational input files (PDF)

AUTHOR INFORMATION

Corresponding Author

Guillaume Maurin − *Institut Charles Gerhardt Montpellier, CNRS/UM/ENSCM, Montpellier 34293, France;* orcid.org/0000-0002-2096-0450; Email: guillaume.maurin1@umontpellier.fr

Authors

Karuppasamy Gopalsamy − *Institut Charles Gerhardt Montpellier, CNRS/UM/ENSCM, Montpellier 34293, France*

Dong Fan − *Institut Charles Gerhardt Montpellier, CNRS/UM/ENSCM, Montpellier 34293, France*

Supriyo Naskar − *Institut Charles Gerhardt Montpellier, CNRS/UM/ENSCM, Montpellier 34293, France;* orcid.org/0000-0002-3690-6483

Yann Magnin − *R&D, OneTech, CSTJF, TotalEnergies, Pau 64018, France;* orcid.org/0000-0002-4603-632X

Complete contact information is available at: https://pubs.acs.org/10.1021/acsaenm.3c00622

Notes

The authors declare no competing financial interest.

ACKNOWLEDGMENTS

The computational work was performed using HPC resources from GENCI-CINES (Grant A0140907613).

REFERENCES

(1) Yu, X.; Catanescu, C. O.; Bird, R. E.; Satagopan, S.; Baum, Z. J.; Lotti Diaz, L. M.; Zhou, Q. A. Trends in Research and Development for CO_2 Capture and Sequestration. *ACS Omega* **2023**, *8*, 11643−11664.

(2) Kabir, M.; Habiba, U. E.; Khan, W.; Shah, A.; Rahim, S.; Rios-Escalante, P. R. D. l.; Farooqi, Z.-U.-R.; Ali, L.; Shafiq, M. Climate change due to increasing concentration of carbon dioxide and its impacts on environment in 21st century; a mini review. *J. King Saud Univ. Sci.* **2023**, *35*, No. 102693.

(3) Piscopo, C. G.; Loebbecke, S. Strategies to Enhance Carbon Dioxide Capture in Metal-Organic Frameworks. *ChemPlusChem.* **2020**, *85*, 538−547.

(4) Nandi, M.; Okada, K.; Dutta, A.; Bhaumik, A.; Maruyama, J.; Derks, D.; Uyama, H. Unprecedented CO_2 uptake over highly porous N-doped activated carbon monoliths prepared by physical activation. *Chem. Commun.* **2012**, *48*, 10283−10285.

(5) Son, W.-J.; Choi, J.-S.; Ahn, W.-S. Adsorptive removal of carbon dioxide using polyethyleneimine-loaded mesoporous silica materials. *Microporous Mesoporous Mater.* **2008**, *113*, 31−40.
(6) Boer, D. G.; Langerak, J.; Pescarmona, P. P. Zeolites as Selective Adsorbents for CO_2 Separation. *ACS Appl. Energy Mater.* **2023**, *6*, 2634−2656.
(7) Sumida, K.; Rogow, D. L.; Mason, J. A.; McDonald, T. M.; Bloch, E. D.; Herm, Z. R.; Bae, T.-H.; Long, J. R. Carbon Dioxide Capture in Metal−Organic Frameworks. *Chem. Rev.* **2012**, *112*, 724−781.
(8) Mahajan, S.; Lahtinen, M. Recent progress in metal-organic frameworks (MOFs) for CO_2 capture at different pressures. *J. Environ. Chem. Eng.* **2022**, *10*, No. 108930.
(9) Chernikova, V.; Shekhah, O.; Belmabkhout, Y.; Eddaoudi, M. Nanoporous Fluorinated Metal−Organic Framework-Based Membranes for CO_2 Capture. *ACS Appl. Nano Mater.* **2020**, *3*, 6432−6439.
(10) Xiang, S.; He, Y.; Zhang, Z.; Wu, H.; Zhou, W.; Krishna, R.; Chen, B. Microporous metal-organic framework with potential for carbon dioxide capture at ambient conditions. *Nat. Commun.* **2012**, *3*, 954.
(11) Zulkifli, Z. I.; Lim, K. L.; Teh, L. P. Metal-Organic Frameworks (MOFs) and their Applications in CO_2 Adsorption and Conversion. *ChemistrySelect* **2022**, *7*, No. e202200572.
(12) Gebremariam, S. K.; Dumée, L. F.; Llewellyn, P. L.; AlWahedi, Y. F.; Karanikolos, G. N. Metal-organic framework hybrid adsorbents for carbon capture − A review. *J. Environ. Chem. Eng.* **2023**, *11*, No. 109291.
(13) Shekhah, O.; Belmabkhout, Y.; Chen, Z.; Guillerm, V.; Cairns, A.; Adil, K.; Eddaoudi, M. Made-to-order metal-organic frameworks for trace carbon dioxide removal and air capture. *Nat. Commun.* **2014**, *5*, 4228.
(14) Bhatt, P. M.; Belmabkhout, Y.; Cadiau, A.; Adil, K.; Shekhah, O.; Shkurenko, A.; Barbour, L. J.; Eddaoudi, M. A Fine-Tuned Fluorinated MOF Addresses the Needs for Trace CO_2 Removal and Air Capture Using Physisorption. *J. Am. Chem. Soc.* **2016**, *138*, 9301−9307.
(15) McDonald, T. M.; Lee, W. R.; Mason, J. A.; Wiers, B. M.; Hong, C. S.; Long, J. R. Capture of Carbon Dioxide from Air and Flue Gas in the Alkylamine-Appended Metal−Organic Framework mmen-Mg_2(dobpdc). *J. Am. Chem. Soc.* **2012**, *134*, 7056−7065.
(16) Healy, C.; Patil, K. M.; Wilson, B. H.; Hermanspahn, L.; Harvey-Reid, N. C.; Howard, B. I.; Kleinjan, C.; Kolien, J.; Payet, F.; Telfer, S. G.; Kruger, P. E.; Bennett, T. D. The thermal stability of metal-organic frameworks. *Coord. Chem. Rev.* **2020**, *419*, No. 213388.
(17) Moumen, E.; Assen, A. H.; Adil, K.; Belmabkhout, Y. Versatility vs stability. Are the assets of metal−organic frameworks deployable in aqueous acidic and basic media? *Coord. Chem. Rev.* **2021**, *443*, No. 214020.
(18) Jiang, L.; Xie, R. Y.; Shi, W. K.; Wu, E. Y.; Li, B.; Zhang, X. J. Water effect on adsorption carbon capture in metal-organic framework: A molecular simulation. *Carbon Capture Sci. Technol.* **2022**, *4*, No. 100061.
(19) Lin, J.-B.; Nguyen, T. T. T.; Vaidhyanathan, R.; Burner, J.; Taylor, J. M.; Durekova, H.; Akhtar, F.; Mah, R. K.; Ghaffari-Nik, O.; Marx, S.; Fylstra, N.; Iremonger, S. S.; Dawson, K. W.; Sarkar, P.; Hovington, P.; Rajendran, A.; Woo, T. K.; Shimizu, G. K. H. A scalable metal-organic framework as a durable physisorbent for carbon dioxide capture. *Science* **2021**, *374*, 1464−1469.
(20) Vaidhyanathan, R.; Iremonger, S. S.; Shimizu, G. K. H.; Boyd, P. G.; Alavi, S.; Woo, T. K. Direct Observation and Quantification of CO_2 Binding Within an Amine-Functionalized Nanoporous Solid. *Science* **2010**, *330*, 650−653.
(21) Zhai, Q.-G.; Bai, N.; Li, S. n.; Bu, X.; Feng, P. Design of Pore Size and Functionality in Pillar-Layered Zn-Triazolate-Dicarboxylate Frameworks and Their High CO_2/CH_4 and C_2 Hydrocarbons/CH4 Selectivity. *Inorg. Chem.* **2015**, *54*, 9862−9868.
(22) Li, X.-Y.; Duan, H.-Y.; He, C. Engineering a Series of Isoreticular Pillared Layer Ultramicroporous MOFs for Gas and Vapor Uptake. *Inorg. Chem.* **2022**, *61*, 17634−17640.
(23) Liu, B.; Shi, J.; Yue, K.-F.; Li, D.-S.; Wang, Y.-Y. Distinct Temperature-Dependent CO_2 Sorption of Two Isomeric Metal−Organic Frameworks. *Cryst. Growth Des.* **2014**, *14*, 2003−2008.
(24) VandeVondele, J.; Krack, M.; Mohamed, F.; Parrinello, M.; Chassaing, T.; Hutter, J. Quickstep: Fast and accurate density functional calculations using a mixed Gaussian and plane waves approach. *Comput. Phys. Commun.* **2005**, *167*, 103−128.
(25) Hutter, J.; Iannuzzi, M.; Schiffmann, F.; VandeVondele, J. cp2k: atomistic simulations of condensed matter systems. *Wiley Interdiscip. Rev. Comput. Mol. Sci.* **2014**, *4*, 15−25.
(26) Perdew, J. P.; Burke, K.; Ernzerhof, M. Generalized Gradient Approximation Made Simple. *Phys. Rev. Lett.* **1996**, *77*, 3865−3868.
(27) Grimme, S.; Antony, J.; Ehrlich, S.; Krieg, H. A consistent and accurate ab initio parametrization of density functional dispersion correction (DFT-D) for the 94 elements H-Pu. *J. Chem. Phys.* **2010**, *132*, No. 154104.
(28) Grimme, S. Accurate description of van der Waals complexes by density functional theory including empirical corrections. *J. Comput. Chem.* **2004**, *25*, 1463−1473.
(29) VandeVondele, J.; Hutter, J. Gaussian basis sets for accurate calculations on molecular systems in gas and condensed phases. *J. Chem. Phys.* **2007**, *127*, No. 114105.
(30) Goedecker, S.; Teter, M.; Hutter, J. Separable dual-space Gaussian pseudopotentials. *Phys. Rev. B* **1996**, *54*, 1703−1710.
(31) Krack, M. Pseudopotentials for H to Kr optimized for gradient-corrected exchange-correlation functionals. *Theor. Chem. Acc.* **2005**, *114*, 145−152.
(32) Hartwigsen, C.; Goedecker, S.; Hutter, J. Relativistic separable dual-space Gaussian pseudopotentials from H to Rn. *Phys. Rev. B* **1998**, *58*, 3641−3662.
(33) Campañá, C.; Mussard, B.; Woo, T. K. Electrostatic Potential Derived Atomic Charges for Periodic Systems Using a Modified Error Functional. *J. Chem. Theory Comput.* **2009**, *5*, 2866−2878.
(34) Yang, Q.; Zhong, C. Molecular Simulation of Carbon Dioxide/Methane/Hydrogen Mixture Adsorption in Metal-Organic Frameworks. *J. Phys. Chem. B* **2006**, *110*, 17776−17783.
(35) Ewald, P. P. Die Berechnung optischer und elektrostatischer Gitterpotentiale. *Annalen der Physik* **1921**, *369*, 253−287.
(36) Mayo, S. L.; Olafson, B. D.; Goddard, W. A. DREIDING: a generic force field for molecular simulations. *J. Phys. Chem.* **1990**, *94*, 8897−8909.
(37) García-Sánchez, A.; Ania, C. O.; Parra, J. B.; Dubbeldam, D.; Vlugt, T. J. H.; Krishna, R.; Calero, S. Transferable Force Field for Carbon Dioxide Adsorption in Zeolites. *J. Phys. Chem. C* **2009**, *113*, 8814−8820.
(38) Potoff, J. J.; Siepmann, J. I. Vapor−liquid equilibria of mixtures containing alkanes, carbon dioxide, and nitrogen. *AIChE J.* **2001**, *47*, 1676−1682.
(39) Horn, H. W.; Swope, W. C.; Pitera, J. W.; Madura, J. D.; Dick, T. J.; Hura, G. L.; Head-Gordon, T. Development of an improved four-site water model for biomolecular simulations: TIP4P-Ew. *J. Chem. Phys.* **2004**, *120*, 9665−9678.
(40) Al-Matar, A. K.; Rockstraw, D. A. A generating equation for mixing rules and two new mixing rules for interatomic potential energy parameters. *J. Comput. Chem.* **2004**, *25*, 660−668.
(41) Peng, D.-Y.; Robinson, D. B. A New Two-Constant Equation of State. *Ind. Eng. Chem. Fundam.* **1976**, *15*, 59−64.
(42) Widom, B. Some Topics in the Theory of Fluids. *J. Chem. Phys.* **1963**, *39*, 2808−2812.
(43) Dequidt, A.; Devémy, J.; Pádua, A. A. H. Thermalized Drude Oscillators with the LAMMPS Molecular Dynamics Simulator. *J. Chem. Inf. Model.* **2016**, *56*, 260−268.
(44) Rappé, A. K.; Casewit, C. J.; Colwell, K. S.; Goddard, W. A., III; Skiff, W. M. UFF, a full periodic table force field for molecular mechanics and molecular dynamics simulations. *J. Am. Chem. Soc.* **1992**, *114*, 10024−10035.
(45) Naskar, S.; Fan, D.; Ghoufi, A.; Maurin, G. Microscopic insight into the shaping of MOFs and its impact on CO2 capture performance. *Chem. Sci.* **2023**, *14*, 10435.

https://doi.org/10.1021/acsaenm.3c00622
ACS Appl. Eng. Mater. 2024, 2, 96−103

(46) Nose, S. A molecular dynamics method for simulations in the canonical ensemble. *Mol. Phys.* **2002**, *100*, 191−198.
(47) Willems, T. F.; Rycroft, C. H.; Kazi, M.; Meza, J. C.; Haranczyk, M. Algorithms and tools for high-throughput geometry-based analysis of crystalline porous materials. *Microporous Mesoporous Mater.* **2012**, *149*, 134−141.
(48) Magnin, Y.; Dirand, E.; Maurin, G.; Llewellyn, P. L. Abnormal CO_2 and H_2O Diffusion in CALF-20(Zn) Metal−Organic Framework Angstropores: Fundamental Understanding of CO_2 Capture. *ACS Appl. Nano Mater.* **2023**, *6* (21), 19963−19971.
(49) Ho, C.-H.; Paesani, F. Elucidating the Competitive Adsorption of H_2O and CO_2 in CALF-20: New Insights for Enhanced Carbon Capture Metal−Organic Frameworks. *ACS Appl. Mater. Interfaces* **2023**, *15*, 48287.
(50) Rajendran, A.; Shimizu, G. K. H.; Woo, T. K. M. The Challenge of Water Competition in Physical Adsorption of CO2 by Porous Solids for Carbon Capture Applications − A Short Perspective. *Adv. Mater.* **2023**, No. 2301730.
(51) Hasan, Md. N; Bera, A.; Maji, T. K.; Mukherjee, D.; Pan, N.; Karmakar, D.; Pal, S. K. Functionalized nano-MOF for NIR induced bacterial remediation: A combined spectroscopic and computational stud. *Inorg. Chim. Acta* **2022**, *532*, No. 120733.
(52) Yan, Q.; Wang, J.; Zhang, L.; Liu, J.; Wahiduzzaman, M.; Yan, N.; Yu, L.; Dupuis, R.; Wang, H.; Maurin, G.; Hirscher, M.; Guo, P.; Wang, S.; Du, J. A squarate-pillared titanium oxide quantum sieve towards practical hydrogen isotope separation. *Nat. Commun.* **2023**, *14*, 4189.

https://doi.org/10.1021/acsaenm.3c00622
ACS Appl. Eng. Mater. 2024, 2, 96−103